Title
Solar energy conversion with photon-enhanced thermionic emission

Journal
Journal of Optics, 18(7)

ISSN
1464-4258

Authors
Kribus, Abraham
Segev, Gideon

Publication Date
2016-07-01

DOI
10.1088/2040-8978/18/7/073001

Peer reviewed

Solar energy conversion with photon-enhanced thermionic emission

2016 J. Opt. 18 073001

(http://iopscience.iop.org/2040-8986/18/7/073001)

IOP Publishing Journal of Optics
J. Opt. 18 (2016) 073001 (18pp) doi:10.1088/2040-8978/18/7/073001

Topical Review

Solar energy conversion with photon-enhanced thermionic emission

Abraham Kribus[1] **and Gideon Segev**[2]

[1] School of Mechanical Engineering, Tel-Aviv University, Tel Aviv 69978, Israel
[2] School of Electrical Engineering, Tel-Aviv University, Tel Aviv 69978, Israel

E-mail: kribus@tauex.tau.ac.il

Received 22 January 2015, revised 28 April 2016
Accepted for publication 29 April 2016
Published 18 May 2016

Abstract

Photon-enhanced thermionic emission (PETE) converts sunlight to electricity with the combined photonic and thermal excitation of charge carriers in a semiconductor, leading to electron emission over a vacuum gap. Theoretical analyses predict conversion efficiency that can match, or even exceed, the efficiency of traditional solar thermal and photovoltaic converters. Several materials have been examined as candidates for radiation absorbers and electron emitters, with no conclusion yet on the best set of materials to achieve high efficiency. Analyses have shown the complexity of the energy conversion and transport processes, and the significance of several loss mechanisms, requiring careful control of material properties and optimization of the device structure. Here we survey current research on PETE modeling, materials, and device configurations, outline the advances made, and stress the open issues and future research needed. Based on the substantial progress already made in this young topic, and the potential of high conversion efficiency based on theoretical performance limits, continued research in this direction is very promising and may yield a competitive technology for solar electricity generation.

Keywords: thermionic emission, solar energy, high-temperature semiconductor, PETE

(Some figures may appear in colour only in the online journal)

1. Introduction

Conversion of sunlight to electricity has been the target of vigorous research and development for many decades, based on the realization that solar energy is the most abundant energy resource on Earth, and its use will mitigate the adverse effects that are attributed to fossil fuels. Solar electricity generation is already implemented on a large scale with both photovoltaic and thermal conversion, but the conversion efficiency of leading technologies in both cases is currently less than 20%. A significantly higher conversion efficiency was achieved with two emerging solar technologies. Concentrator photovoltaic systems (CPV) with multi-junction cells offer a peak cell-level efficiency of over 40%, and a system-level efficiency (including optical and other losses) of over 30% [1]. Solar thermal Dish-Stirling concentrator systems have also achieved over 30% system efficiency [2]. However, these two technologies are not in widespread use due to their higher complexity and cost compared to the more mature but less efficient alternatives.

Recently, a third approach has been proposed for high-efficiency conversion of sunlight to electricity: photon-enhanced thermionic emission (PETE), which is based on the emission of electrons from a hot semiconductor surface, assisted by direct photonic excitation in the semiconductor. A synergy of optical and thermal excitation was first demonstrated experimentally by Smestad [3], where combined heating and illumination produced higher electrical output than the sum of the separate outputs of heating and illumination only. He proposed that the effect is due to the emission of hot electrons. Schwede *et al* [4] suggested the PETE mechanism based on thermalized rather than hot electrons,

and have experimentally shown that the emitted electrons follow a thermal distribution independent of the energy of the incident photons, confirming that they are thermalized. Schwede *et al* also presented a model of the PETE process with estimates of high PETE conversion efficiency, e.g. efficiency exceeding 43% for incident solar radiation concentration of ×1000 and cathode temperatures below 1000 °C. The conversion efficiency of a PETE device under concentrated solar radiation can therefore exceed, at least theoretically, the efficiency of a single-junction photovoltaic cell under the same concentration. When adding the option of a second stage thermal converter that uses heat removed from the anode, the overall efficiency can reach above 53% and theoretically compete against the best multi-junction cells developed for the CPV industry. Later theoretical models set the upper limit on ideal PETE converter efficiency at a concentration of ×1000 above 50%, and at 70% with the addition of an ideal bottoming converter that utilizes waste heat [5]. If real devices could reach close to these theoretical limits, then the PETE approach may be competitive against the two existing conversion methods. Therefore, this new path to the generation of electricity from sunlight has raised considerable interest, and the first steps are underway towards understanding and implementing PETE converters.

The emission of electrons from a solid surface can be induced by the addition of energy, using either incident radiation (photo-emission), an externally applied voltage (field emission), or externally supplied heat (thermionic emission). Thermionic emission of electrons from heated metals was observed during the second half of the 19th century by several researchers [6], and was later described quantitatively by Richardson [7]. A brief historical review of thermionic emission research can be found in [8]. A thermionic emitter converts thermal energy to electrical energy, equivalent to a heat engine, but without the need for mechanical moving parts. A basic thermionic converter typically contains an electron emitter (cathode) at high temperature, and an electron collector (anode) at a lower temperature. The gap between the two electrodes is in a vacuum or filled with a gas at low pressure. The cathode emits electrons from its surface, and the anode captures the electrons to create an electrical current. The converter further includes external electrical connections that allow the circuit to be closed through an external load, and two heat sinks to provide heat to the cathode and remove waste heat from the anode.

The current density of electron emission from a metal typically behaves according to the Richardson–Dushman equation [9]:

$$J = \lambda A_0 T_C^2 e^{-\phi_C/kT_C} \tag{1}$$

$A_0 = 120$ A cm^{-2} K^{-2} is the Richardson–Dushman constant, λ is a material dependent correction, k is Boltzmann's constant. The current density increases non-linearly with cathode temperature T_C, but most cathode materials have high values of the work function ϕ_C, and therefore very high temperatures are needed to increase the exponential term and generate a significant current. Thermionic converters typically require cathode temperatures over 1000 °C, and often close to 2000 °C. The current of a thermionic converter is the net current after subtraction of the reverse emission of electrons from the anode, but the anode is usually much cooler and its emission current is usually neglected. In order to produce power, the converter must also produce a positive voltage, and this is achieved when the anode work function ϕ_A is lower than the cathode work function ϕ_C.

The development of thermionic converters was a popular research topic until the 1970s, with theoretical predictions of conversion efficiency above 30% [10]. Significant hopes for practical application were raised after the discovery that introducing low-pressure cesium vapor in the inter-electrode gap improves the performance of a thermionic converter [11]. Many applications were envisioned where the heat source could be the combustion of fuel, concentrated solar radiation, decay of radio-isotopes, or coolant from a nuclear fission reactor. However, the achieved conversion efficiency from heat to electricity was usually around 10% even at very high cathode temperatures [6]. The high expectations were then not realized, and interest in thermionic energy converter technology has since declined.

PETE is a combination of two mechanisms for electron emission—thermal and photonic—working together in synergy [4]. In PETE conversion, the cathode is illuminated by an external source such as concentrated solar radiation, as shown in figure 1(a). Photons with energy above the cathode material's bandgap are absorbed and generate electron-hole pairs. The optically generated electrons thermalize in the conduction band, increase the conduction band electron population, and raise the conduction band quasi-Fermi level. As a result, the energy barrier for electron emission to the vacuum is reduced, as shown in figure 1(b), allowing electron emission at temperatures considerably lower than standard thermionic emission (figure 1(c)). Excess photon energy above the bandgap is converted to thermal energy by thermalization, and sub-bandgap photons may also contribute to the heating of the cathode, if it contains some means to absorb these photons. Both of these mechanisms keep the cathode at an elevated temperature without the need for an additional heat source. Therefore, PETE conversion involves a combination of both photonic and thermal conversion of the incident radiation.

Another interesting aspect of PETE converters is the ability to keep the anode at a temperature high enough for waste heat utilization, but not so high as to create a significant reverse current. The waste heat removed from the anode can then be used to generate additional electricity in a second stage thermal converter, similar to a combined cycle (CC) in conventional thermal power plants. The overall conversion efficiency from the incident radiation to the output electrical power is then increased by adding this second stage conversion.

These promising ideas have led to a recent revival of interest in electron emission and PETE for solar energy conversion, with considerable theoretical and experimental research activities in many groups around the world. The

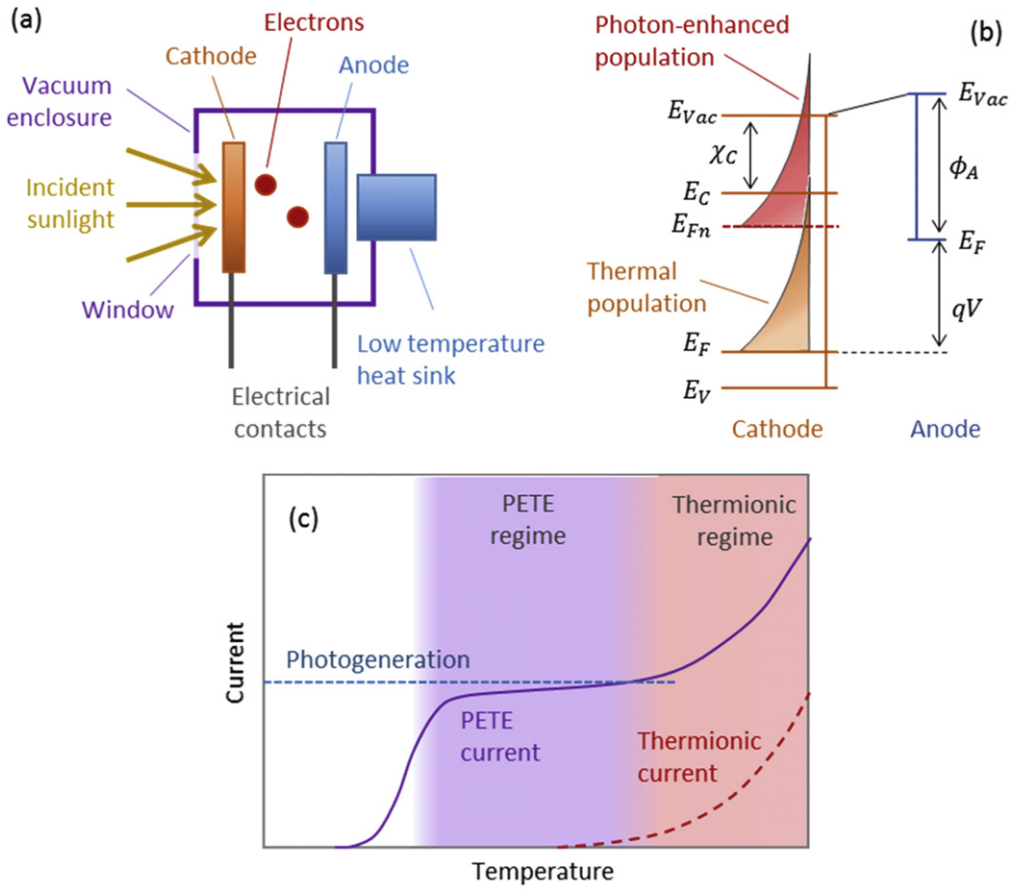

Figure 1. (a) Layout of a basic PETE converter, where the cathode is illuminated and heated with concentrated solar radiation. (b) Energy band diagram, showing that illumination of the semiconductor cathode raises the electrons' quasi-Fermi level and reduces the energy barrier for emission (adapted from [4]). (c) Enhancement of emission current at moderate temperatures due to photonic excitation in PETE (adapted from [4]).

present review addresses the directions and initial results of these efforts over the last five years.

2. Models and performance

2.1. Simple modeling of converter physics

The simplest analysis of PETE converters is an ideal particle balance, as commonly done for photovoltaic cells [12]. It treats the cathode as a lumped system with averaged properties and no spatial variations, and therefore can be called a zero-dimensional model. The cathode absorbs all the above band gap radiation (optically thick); usually, only radiative recombination is considered (perfect cathode material). The anode is metallic and is perfectly reflective (radiative loss occurs only through the front surface), and space charge in the inter-electrode gap is ignored (this is discussed in section 2.4 below). Under such assumptions, the net current is the difference between the total optical generation G and the non-equilibrium recombination R' [4]:

$$qW(G - R') = (J_{em} - J_{rev})S \tag{2}$$

q is the electron charge, J_{em} and J_{rev} are the emission current densities from the cathode and anode surfaces, respectively. S is the ratio of the area for electron emission to that of radiation absorption, which is 1 for the standard configuration shown in figure 1(a). The emission current density from the cathode is proportional to the electron concentration n and can be expressed as [4]:

$$J_{em} = qn\left(\frac{qkT_C}{2\pi m_m}\right)^{1/2} e^{-E_{BC}/kT_C} \tag{3}$$

m_m is the electron effective mass. The energy barrier for emission from the cathode E_{BC} equals the electron affinity χ for device voltage below the 'flat band voltage' (the highest voltage where all emitted electrons can reach the anode): $qV < \phi_C - \phi_A$, where ϕ_C and ϕ_A are the work function of the cathode and anode. In this range, the electric field in the gap (in the absence of space charge) accelerates the emitted electrons towards the anode, as shown in figure 2(a). For higher voltage, the vacuum level at the anode is higher than that of the cathode; the direction of the electric field is reversed, and the barrier is $E_{BC} = \phi_A + qV - \phi_C$ as seen in figure 2(b). The reverse emission current density from the anode follows the standard thermionic emission formulation:

$$J_{rev} = \lambda A T_A^2\, e^{-E_{BA}/kT_A} \tag{4}$$

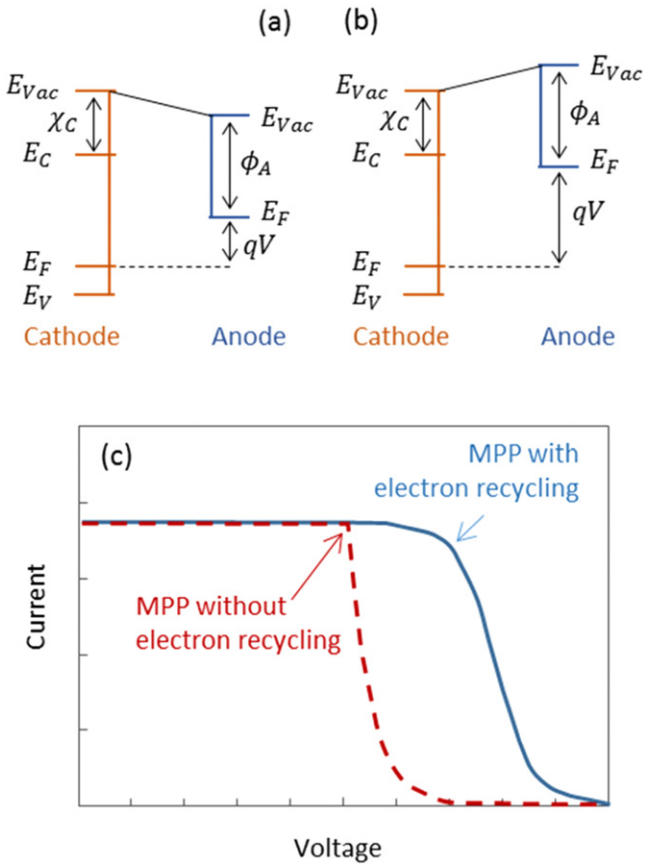

Figure 2. (a) Energy levels diagram of an ideal PETE converter at voltage below the flat band voltage. (b) Band diagram at voltage higher than the flat band voltage. (c) Illustration of current-voltage curves for the models with and without electron recycling at the cathode.

T_A is the anode temperature. The energy barrier for emission from the anode equals the anode work function ϕ_A for voltage above the flat band value, and $E_{BA} = \phi_C - qV$ for lower voltage (figure 2). The PETE converter efficiency can then be evaluated by inserting the appropriate generation and recombination terms into equation (2) along with the current density terms from equations (3) and (4), and scanning the device voltage range to identify the maximum power point (MPP) voltage V_{MPP}:

$$\eta = \frac{[J_{em}(V_{MPP}) - J_{rev}(V_{MPP})]\, V_{MPP}}{P_{sun}} \tag{5}$$

P_{sun} is the flux density of concentrated radiation incident on the PETE converter. The MPP voltage for this simple model is the flat band voltage $V_{MPP} = (\phi_C - \phi_A)/q$, as seen in figure 2(c) [4]. Achieving a high device voltage requires that the Fermi level should be near the bottom of the bandgap, i.e. the cathode should be a p-type semiconductor.

In contrast to metallic cathodes, the electron concentration n in a semiconductor cathode can depend on the device voltage: above the flat band voltage, electrons that are reflected by the higher barrier have sufficient energy to recycle, i.e. return to the cathode conduction band. These recycled electrons increase the electron concentration in the cathode, and can re-emit to the vacuum or be recombined, similar to any other electron already present in the conduction band [13]. It is not known what fraction of these reflected electrons actually enters the conduction band, versus the fraction that may undergo immediate recombination at the surface and have no effect on the state of the cathode. The significant impact of surface recombination at the emitting surface was shown both theoretically [14, 15] and experimentally [16], so the interaction of electron recycling with surface recombination should be considered. However, these investigations referred to the recombination of electrons already present in the cathode's conduction band, and do not provide the much needed insight about the fate of the reflected electrons. Analyses that assume perfect electron recycling (all reflected electrons enter the conduction band) [13], show a distinct difference in the behavior of the current above the flat band voltage, compared to analyses that assume no electron recycling (recombination of all reflected electrons at the surface), as seen in figure 2(c). This leads to a change of the MPP to higher voltage, and to the prediction of higher output power and higher efficiency.

The cathode temperature is determined by a complete energy balance on the cathode, including absorption of incident radiation, electron transport to the anode, and radiative and conductive loss to the environment [17, 18]. Ideally, conduction loss is zero and this leads to the maximum attainable cathode temperature. An ideal cathode in principle may absorb only supra-bandgap radiation, but it has been proposed that adding an element in the cathode that also absorbs sub-bandgap radiation can increase its temperature and contribute to higher electron emission [4]. However, this will also increase the loss by the emission of blackbody radiation, so this element needs to be carefully optimized.

The waste heat to be removed from the anode of the PETE converter is the thermalization energy of electrons entering the anode, $(J_{em} - J_{rev})E_{BA}$. An ideal second stage will convert this heat to electricity at the Carnot efficiency corresponding to the anode temperature, adding to the total conversion efficiency of a PETE converter operating as a CC.

2.2. Elaborated models

Elaborated models of a PETE converter account for the spatial distribution of the cathode properties, the charge carrier concentrations and the electric potential, and allow internal structures such as junctions. Several levels of complexity are possible in formulating an elaborate model. A simple model used a one-dimensional diffusion equation to describe the transport of excess electrons in a p-type cathode [15, 14]:

$$D_n \frac{d^2 n}{dx^2} = \frac{n - n_{eq}}{\tau_n} - G(x) \tag{6}$$

D_n is the electrons diffusion coefficient, τ is the electron lifetime. This assumes that photo-generated electrons are fully thermalized, and that low injection and charge neutrality are maintained, so that the electric field in the cathode is negligible. Under these conditions the transport of electrons is dominated by diffusion and uncoupled from the transport of

holes. This approximation is valid in a p-type cathode as long as the higher concentration of majority carriers (holes) is able to neutralize any charge imbalances that could produce a significant field. In high injection conditions, this may not hold because the concentration of minority carriers is not negligible compared to majority carriers, and a more general treatment is needed as discussed below. Another exception is an intrinsic rather than a p-doped absorber [19], where a version of the diffusion model was used with two separate equations for the transport of electrons and holes.

The generation profile can be represented according to two-pass absorption of collimated radiation [14]:

$$G(x) = \int_0^\infty \Phi \cdot \alpha(1 - \rho_F)[e^{-\alpha x} + \rho_B e^{-\alpha(2W-x)}]\mathrm{d}\lambda \quad (7)$$

Φ is the spectral flux of incident radiation, α is the absorption coefficient ($\alpha = 0$ for photon energy below the material's bandgap), ρ_F and ρ_B are the reflection coefficients of the front and back surfaces (single-pass generation is obtained when $\rho_B = 0$ [15]), and t is the cathode thickness. More sophisticated optical models are needed to represent the directional spread of incident radiation due to concentration, and the effect of surface structures that reduce reflection [20]. The electron lifetime that represents all forms of recombination is related to the electron diffusion coefficient D_n and the electron diffusion length L_n : $D_n\tau_n = L_n^2$, and it is usually taken as a constant [15]. The constant lifetime assumption simplifies the analysis, and is a good approximation under low injection. Under high injection conditions and over a wide range of temperatures this is not a valid approximation [21], and each recombination mechanism should be modeled in detail, including explicit dependence on charge carrier concentration and on temperature [22].

The coordinate x extends from the front face of the cathode (exposed to the incident radiation, $x = 0$) to the emitting surface at the back ($x = t$), with boundary conditions that represent electron emission and surface recombination [14]:

$$\begin{aligned} D\frac{dn}{dx}\bigg|_0 &= S_{n,F}[n(0) - n_{eq}(0)] \\ -D\frac{dn}{dx}\bigg|_t &= S_{n,B}[n(t) - n_{eq}(t)] + \frac{J_{em} - J_{rev}}{q} \end{aligned} \quad (8)$$

$S_{n,F}$ and $S_{n,B}$ are the surface recombination velocities at the front and back surfaces, respectively. The model of equations (6)–(8) can be solved analytically for the electron emission yield [15], and for the output power and efficiency using either the flat band voltage, or a numerically optimized voltage [14]. These solutions were used to investigate the influence of important parameters including the cathode thickness, surface recombination velocities, and electron affinity at the emitting surface.

The electron diffusion model described above provides a fast and flexible tool to investigate many aspects of PETE conversion. However, the simplifying assumptions of this model do not hold in some situations. At a sunlight concentration of 1000 or higher, the low injection approximation may become invalid. Internal junctions and surface treatments in the cathode may induce band bending and a locally high electric field that affects charge carrier transport, as shown for example in [18]. In some cases, an approximate treatment of a junction can be added within the diffusion model [23] to avoid the computational cost of more complex models. A more general model for the PETE cathode that does not need the simplifying assumptions uses the general description of transport in semiconductors. The governing equations include the continuity equations that describe the charge carriers' transport, and Poisson's equation for the potential, as a function of position $\vec{x}$ in one or more dimensions [22]:

$$\nabla \cdot \vec{J}_n(\vec{x}) = -q[G(\vec{x}) - R(\vec{x})] \quad (9)$$

$$\nabla \cdot \vec{J}_p(\vec{x}) = q[G(\vec{x}) - R(\vec{x})] \quad (10)$$

$$\nabla \cdot (\epsilon\, \vec{\nabla}\Psi) = q[N_A^-(\vec{x}) - N_D^+(\vec{x}) + n(\vec{x}) - p(\vec{x})] \quad (11)$$

$\vec{J}_n$ and $\vec{J}_p$ are the electron and hole current densities, respectively, including the contributions due to drift and diffusion; G and R are the rates of generation and total recombination per unit volume, respectively. ϵ is the permittivity, N_A^- and N_D^+ are the concentrations of ionized acceptors and donors, respectively. The current densities in the continuity equations are defined in terms of the electron and hole concentrations $n(\vec{x})$, $p(\vec{x})$, and the quasi-Fermi potentials for holes and electrons [22]. The generation function $G(\vec{x})$ can follow equation (7), or a more detailed optical model if available. The recombination term $R(\vec{x})$ is the sum of radiative, Auger and SRH recombination rates and should be calculated for each location using the respective general expressions as found, e.g. in [22], including the non-linear dependence on carrier concentration and on temperature. The boundary conditions are analogous to equation (8), duplicated for both holes and electrons [18], and applied to the component of charge carrier transport in the direction of the surface normal $\hat{n}$: $\hat{n} \cdot \vec{J}_n$ and $\hat{n} \cdot \vec{J}_p$ for electrons and holes, respectively. For the potential, it is convenient to apply a zero value at the cathode contact, and a Neumann type boundary condition on the electric field at the electron emission surface, which depends on the applied device voltage [18]. When the cathode structure includes a hetero-junction, the material properties in equations (9)–(11) will have a discontinuity, and internal continuity conditions need to be applied at the junction interface [22].

The more general model with equations (9)–(11) has been solved for cases where the simplified diffusion equation treatment is insufficient, including a one-dimensional slab geometry with internal junctions [18] and for two-dimensional geometry [24]. It should be noted that in both modeling approaches described above, there is no treatment of photon recycling: photons that are emitted internally due to radiative recombination are considered as lost, even though some of them are reabsorbed in the cathode and generate new electron-hole pairs. Modeling of this effect will add considerable complexity and has not been attempted yet.

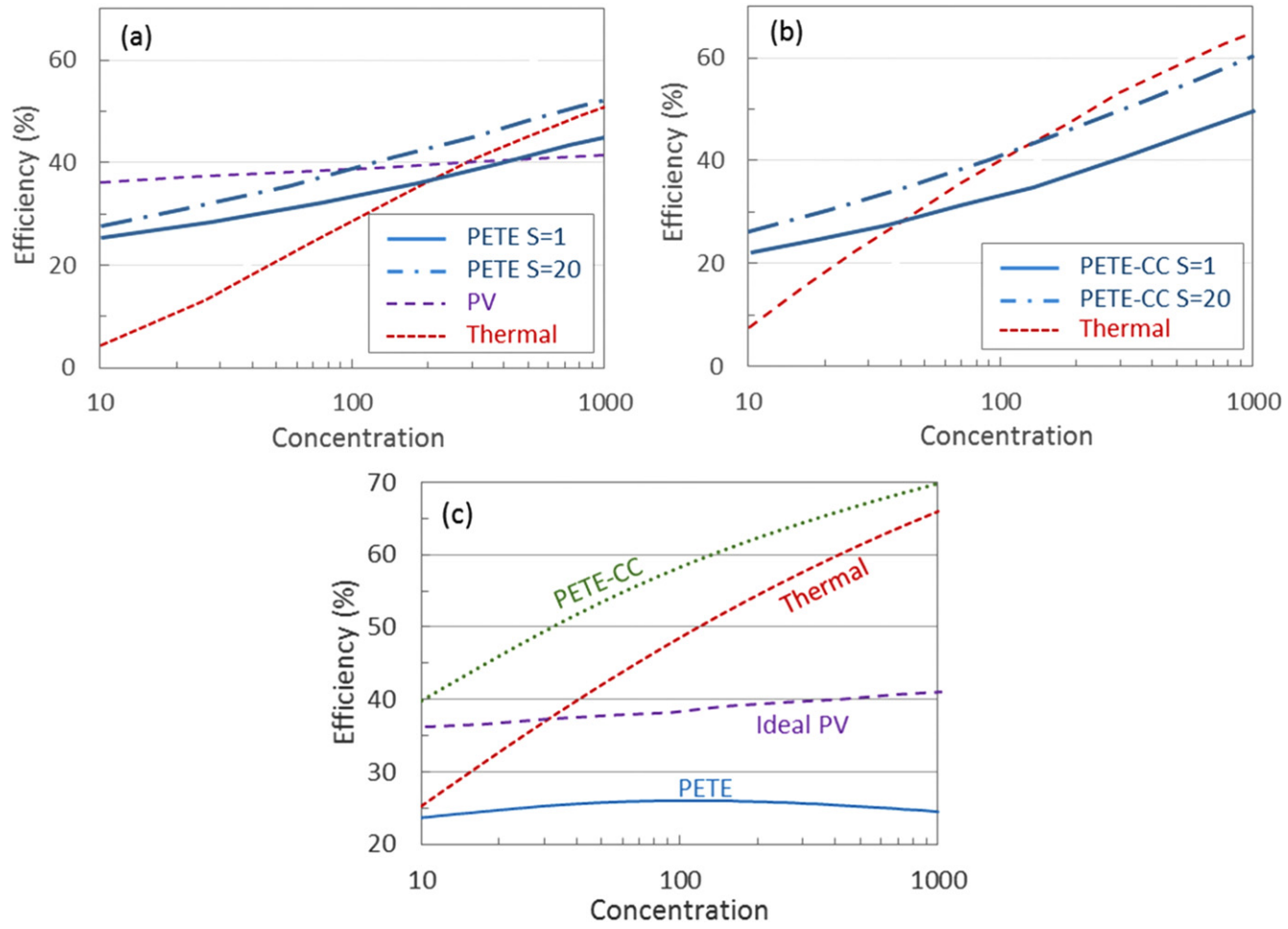

Figure 3. (a) Efficiency of ideal PETE, ideal thermal, and ideal PV converters as a function of the flux concentration. S is the cathode area ratio, defined in equation (2). (b) Efficiency of ideal PETE combined cycle (PETE-CC) with a secondary thermal stage, compared to an ideal thermal converter, as a function of the flux concentration. The cathode is doped 10^{19} cm^{-3} p-type with a band gap 1.4 eV and electron affinity 0.4 eV; the anode work function is 0.9 eV and its temperature is 500 K. (c) Efficiency of isothermal tandem PETE with and without an ideal secondary thermal converter, compared to an ideal photovoltaic converter (SQ limit) and an ideal thermal converter. (Adapted from [5]).

2.3. The efficiency limits of a PETE converter

The efficiency limit is derived with a simplified model, where only inevitable loss mechanisms are applied, and material properties can have any value regardless of the availability of real materials. This was done in several published analyses using the particle balance zero-dimensional model. First results placed this theoretical efficiency at about 43% at 1000 suns, with an optimal choice of bandgap and electron affinity [4]. Other analyses made some variations regarding the included losses, for example, including heat exchange between the cathode and anode, leading to lower efficiency values, e.g. 0.38 at 1000 suns with the optimal bandgap and affinity [17].

A detailed study of the PETE converter efficiency limit as a function of the concentration of the incident solar radiation in comparison to ideal PV and thermal conversion was reported in [5]. The cathode temperature was the maximum allowed by the energy balance, and the anode temperature was fixed at 500 K. Figure 3(a) shows the resulting PETE efficiency versus the efficiencies of an ideal photovoltaic cell calculated according to the Shockley–Queisser (SQ) derivation [12], and an ideal solar thermal converter comprising a black absorber and an ideal Carnot engine with a cold reservoir temperature of 500 K [25]. At a high concentration and high cathode temperature the PETE efficiency exceeds the ideal photovoltaic cell efficiency, reaching 45% at a concentration of 1000. With the high cathode area ratio $S = 20$ (see equation (2), higher area for electron emission) the radiative recombination loss is reduced, and the PETE efficiency also exceeds the ideal thermal converter, reaching 52% at a concentration of 1000. It should be stressed that these high efficiencies are obtained when the cathode temperature is at the theoretical maximum, with only blackbody emission loss to the environment, and this temperature is 1300 K or higher at 1000 suns [5]. This is outside the range of operation of most semiconductors, so the performance limit seems out of reach for practical devices.

Figure 3(b) shows the efficiency of a PETE combined cycle, where the second stage is an ideal Carnot engine operating at the anode temperature. The PETE-CC efficiency limit is higher due to the contribution of the second stage,

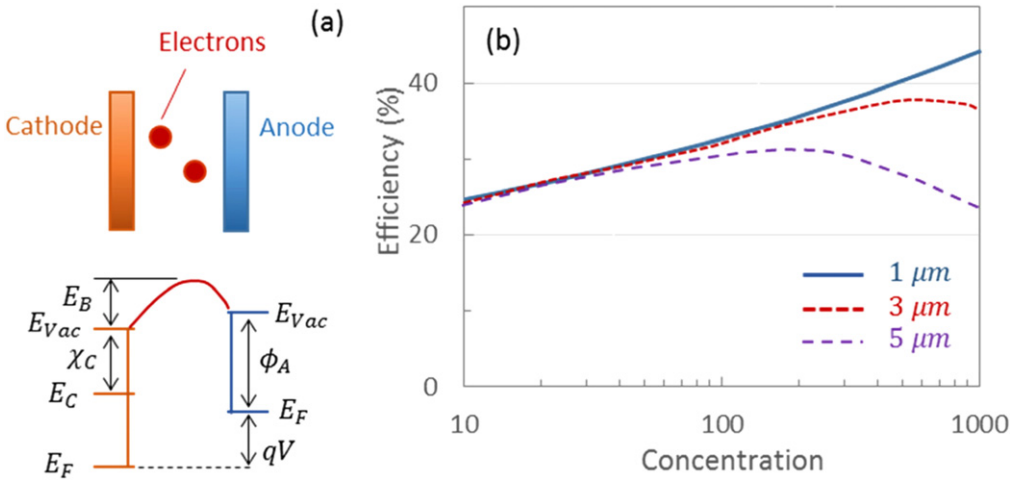

Figure 4. (a) Schematic of the negative space charge location and energy diagram. (b) Efficiency of a PETE converter with NSC effect, for different values of the gap width (adapted from [34]).

reaching 56% and 63% for the cathode aspect ratio of 1 and 20, respectively. Similar CC configurations were explored for CPV cells, but their performance was lower due to a decline in cell efficiency with temperature [26]. An analysis of a CC with an optimized cathode but a specific non-ideal second stage converter (thermoelectric) predicted a relatively small contribution of the second stage, and overall efficiency of about 46% at a concentration of 1000 [27], well below the upper limit.

A different approach is to optimize the efficiency of a PETE-CC by minimization of entropy generation [28]. The best efficiency prediction at 1000 suns is 58%, and 60.8% in a CC configuration with an ideal secondary heat engine. However, this solution requires a cathode at 1451 K, a very low bandgap (0.56 eV), and zero chemical potential, i.e. it is essentially a thermionic converter without photonic enhancement. Also, the anode temperature is 328 K, so that the second stage contributes very little. This unusual solution may be a result of not using an IR absorber in the cathode, forcing the bandgap to a low value in order to absorb most of the solar spectrum, and then compensating with a high electron affinity (to obtain useful voltage) and high temperature (to overcome the high affinity). Additional solutions presented in [28] show a bandgap about 1 eV and non-zero chemical potential (indicating photonic enhancement) of 0.28 eV, but they offer efficiency below 45%, even though they require a cathode temperature above 1450 K. Possibly a more practical solution is also shown with a cathode temperature of 573 K, a bandgap of 0.82 eV, and an efficiency of 37.9% (44% with an ideal secondary heat engine), which is impressive for this low temperature. It is interesting to note that these solutions tend to recommend lower optimal bandgaps compared to other analyses (e.g. about 1.4 eV in [4]). This seems to be due to the allowance of a very low anode work function (0.41 eV), which enables reasonable device voltage with these lower bandgaps. This, however, also forces low anode temperatures to prevent high reverse emission, leading to a low contribution of the secondary stage to the overall efficiency.

The analysis of conversion efficiency reveals what material properties are needed to obtain high efficiency, as a guideline to search for suitable real materials. Most of the results show that the optimal bandgap of the cathode is around 1.4 eV, similar to the optimum for PV cells, a result dictated by the solar spectrum. Observation of figures 2(a) and (b) reveals that in order to obtain a reasonable output voltage, the cathode work function should be significantly higher than that of the anode. So, the anode work function should be low, and the cathode Fermi level should be low, i.e. high p-type doping. The cathode electron affinity should be low to allow high current density; however below a certain value (e.g. $\chi = 0.7$ eV for concentration 1000 and $T_C = 773$ K), the efficiency is not sensitive to the affinity value [13]. An analysis without electron recycling shows a very different dependence on electron affinity, with an optimal value below which the efficiency declines [4]. The former trend seems to be physically correct, since the barrier that cathode electrons need to overcome is determined by the anode vacuum level (and space charge if present), and a reduction of the cathode electron affinity to very low values should not have an effect.

Tandem, or multi-junction, configurations are well known in photovoltaic conversion, where several sub-cells with different bandgaps produce a better coverage of the solar spectrum. This may also work theoretically for PETE tandem converters, leading to 51.2% theoretical efficiency for a two-bandgap device under 1000 suns [5]. The improvement compared to the single-bandgap converter is not dramatic, since PETE already utilizes some of the thermalization energy, and its reduction by spectral splitting is less significant compared to PV cells. Another tandem approach is to join identical sub-cells electrically in series to create a high-voltage, low-current device and reduce Ohmic losses [29], similar to the vertical multi-junction configuration that has been proposed for PV cells [30]. The converter is isothermal and the driving mechanism is only the photonic excitation of the cathode, leading to efficiency below the SQ limit, as shown in figure 3(c). A secondary thermal converter collects

waste heat from the cathodes as well as from the anodes, leading to a higher contribution by the secondary stage, and combined efficiency exceeding both ideal photovoltaic and ideal thermal converters, reaching 70.4% at a concentration of 1000 [5].

2.4. Negative space charge

Negative space charge (NSC) is a well-known effect in thermionic emission. The electrons emitted from the cathode form a negatively charged electron cloud in the inter-electrode space, as shown in figure 4(a). This negative space charge may produce an added energy barrier (E_B in the figure) that impedes emitted electrons from reaching the anode. The loss inflicted by NSC is high in thermionic converters [31]. The behavior of the space charge can be described with a model that couples the electron transport in the gap to the electron emission current from the cathode. The electrons in the gap can be described as one-dimensional transport of a collisionless gas [9]. The potential distribution in the gap can be obtained following the analysis of Langmuir [32]. Analysis of the NSC effect using this model for PETE converters has shown a sharp decline in efficiency as the gap size increases, similar to thermionic converters. At a sunlight concentration of 1000 and a cathode temperature of 1000 K, the predicted efficiency was about 24%, 19% and 15% for gaps of 2 μm, 3 μm, and 4 μm, respectively [33].

When assuming electron recycling in the cathode, the reflection of electrons by the NSC effect increases the conduction band population and increases the rate of electron emission, mitigating some of the decline in efficiency [34]. It was shown that for a selected test case, full electron recycling can approximately double the efficiency for the presented gap sizes of 2 μm and 5 μm compared to results with no electron recycling, allowing larger gaps to become acceptable. The NSC effect was also investigated as a function of sunlight concentration, as shown in figure 4(b). For a moderate sunlight concentration of around 100, even a gap of 5 μm can maintain reasonable efficiency, but at higher concentrations approaching 1000, the gap must shrink to 3 μm or less [35]. The cathode is at ideal thermal equilibrium, i.e. the highest temperature allowed by the given concentration. In figure 4(b), it is also clear that for a converter with a specific gap, there is an optimal solar flux concentration. The technological ability to fabricate a small gap then influences a separate decision on the concentration optics.

Several methods were proposed to reduce the performance loss due to NSC in thermionic and PETE converters. Reducing the gap between the electrodes to a few microns diminishes the amount of electrons present in the gap, and with it the energy barrier and the performance loss, as discussed above. However, the gap should not be too small: below about 1 μm, near field radiation heat transfer between the two electrodes can reduce the converter efficiency [35]. Such small gaps may be produced with microfabrication methods [36] or by insertion of very small spacers [37]. Another approach to reduce the negative space charge loss is to introduce positive charges in the gap, which cancel the effect of the negative charge, for example filling the gap with low pressure cesium vapor [6]. Denser plasma can be formed by optically exciting the cesium, lowering its effective ionization potential and canceling the NSC more effectively [38]. Methane also reduces the negative space charge loss in a similar manner, and introduces molecular charge transport as well [39]. Incorporation of a positively charged grid between the two electrodes to accelerate the emitted electrons can also reduce NSC loss [40]. Using negative electron affinity cathodes is also beneficial, as the emitted electrons leave the cathode with energy higher than the vacuum level at the surface, and have a higher probability of overcoming the NSC energy barrier [41].

2.5. Predicted performance of real PETE converters

Realistic predictions of PETE converter performance employ an elaborated cathode model, with optical and electronic properties of real materials and their variation with temperature, and realistic boundary conditions including surface recombination. The performance then depends on many cathode material properties, including bandgap, absorption coefficient, doping level, diffusion length, lifetime, electron affinity, bulk recombination rates, and on surface recombination velocities, on cathode thickness and on the concentration of incident sunlight and cathode temperature. Studies published so far only partially cover this extensive parameter space.

The effect of surface recombination has been investigated in several cases. The emission yield of a GaAs cathode for moderate temperatures declines significantly when recombination velocity at the back surface (electron emission surface) increases from 10^3 cm s^{-1} to 10^6 cm s^{-1} [15]. At higher temperatures the thermionic emission dominates over the surface recombination, e.g. emission yield approaches 1 at 600 °C for surface recombination velocities up to 10^5 cm s^{-1}. The conversion efficiency for a Si cathode was shown to decline from about 15% at 800 K with zero recombination at the back surface, to about 10% if the back surface recombination velocity is 10^3 cm s^{-1} [14]. A method to reduce the recombination loss at the back surface is to add a hetero-junction that forms a small energy barrier, allowing only energetic electrons to reach the electron emission surface [16]. This was modeled and also demonstrated experimentally on a cesiated GaAs cathode with an internal quantum efficiency (QE) of 1.4% at 120 °C, and close to 1 when extrapolated to 600 °C, as shown in figure 5(a).

A study of Si and GaAs cathodes found that recombination at the front surface (surface with incident radiation and electrical contact) also creates a significant loss [18]. Insertion of a p^+p homojunction at the front surface below the contact was only partially successful to mitigate the effect of surface recombination due to the decrease in barrier height as the temperature increases. The predicted efficiency for both materials was limited to around 15% at moderate temperatures. A better solution is a hetero-junction at the front surface serving as a window layer. Figure 5(b) shows the predicted efficiency for a GaAs cathode with a AlGaAs window, both

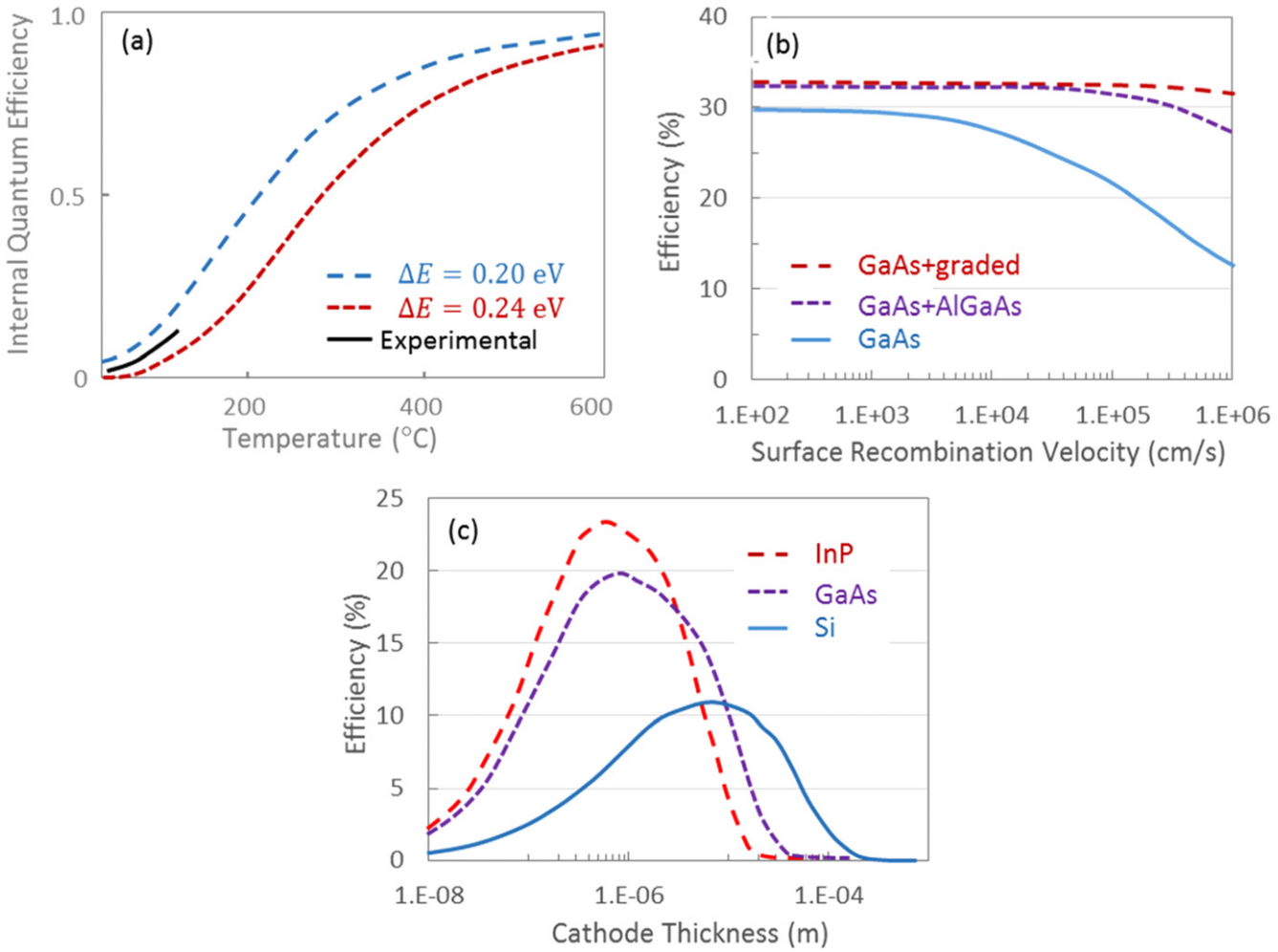

Figure 5. (a) Internal quantum efficiency for a cesiated GaAs cathode with a hetero-junction barrier at the back surfaces, experimental results up to 120 °C and model predictions up to 600 °C (adapted from [16]). (b) Efficiency of a GaAs cathode with AlGaAs window layers, abrupt and graded, as a function of window surface recombination velocity (adapted from [23]). (c) Predicted conversion efficiency for SI, GaAs, and InP cathodes at 1000 suns and 700 K, as a function of cathode thickness (adapted from [21]).

as an abrupt junction [42] and with graded composition [23]. Both heterojunctions show a higher efficiency of 32% compared to a simple cathode without a junction at 30%, even when recombination at the window surface is negligible, due to the higher voltage produced by the junctions. For higher recombination at the surface, the simple cathode deteriorates quickly, while the junctions maintains a high efficiency of up to 10^5 cm s^{-1} for the abrupt junction and 10^6 cm s^{-1} for the graded junction. In addition, the energy barrier of a hetero-junction does not degrade with temperature, preventing the decline of efficiency with temperature that was observed with a homojunction [18].

The behavior of a contact surface is different at high temperatures: the cathode electron concentration falls below equilibrium, similar to conventional thermionic cathodes, and electrons are then injected from the contact rather than recombined. At the highest temperature allowed by the energy balance under 1000 suns, the predicted efficiencies are 31% at 820 K for Si and 32% at 1080 K for GaAs [18]. A cathode able to operate at such temperatures needs no protection against surface recombination at the contact. The operation of PETE converters can then be divided into two distinct regimes with different behavior: the PETE regime at low and moderate temperatures, where photo-generation makes a significant contribution and electron concentration is above equilibrium; and the thermionic regime at high temperatures, where thermal excitation and emission is dominant and electrons concentration is below equilibrium.

Cathode thickness is a crucial parameter for device design. A thin cathode will collect most of the photo-generated charge carriers, leading to high emission internal yield close to 1 if surface recombination velocities are low [15]. However, low absorption of incident radiation will lead to low efficiency, requiring a thick cathode. Therefore, for each set of material properties there is an optimal cathode thickness that provides the best balance of the two effects. Figure 5(c) shows the variation of conversion efficiency with cathode thickness for three materials at 1000 suns and 700 K [21]. For Si the cathode thickness should be around 7 μm and the predicted efficiency is 11%, consistent with previously cited low values. For GaAs and InP the optimal thickness is a few hundred nm, due to the much higher absorption coefficient,

and the conversion efficiency is 20% and 23%, respectively. Clearly the efficiency is very sensitive to the selection of cathode thickness, requiring optimization for each set of material properties.

Most models use the expression (3) for the emission current density from the cathode. However, this should be modified with an emission probability, indicating that electrons having sufficient energy to reach the vacuum may still fail to do so. Measurement of the emission probability for a GaAs with CsO coating show that at the best coating coverage ratio (about 0.4 of a monolayer), emission probability is 12% for thermalized electrons, and 24% for hot electrons [43]. The authors suggest that this is due to fundamental effects that are inherent to any emitting surface, such as electron scattering at the semiconductor–vacuum interface, the influence of an interface potential barrier, or a low probability of a conversion of a Bloch electron in the crystal into a free electron in vacuum. The theory leading to equation (3) is then oversimplified, and a more accurate description of the semiconductor–vacuum interface leads to lower values of the current density. Another experiment with an AlGaAs emission layer coated by CsO showed that a similarly defined emission probability is approximately 0.25 [16]. Obviously, this leads to a significant reduction in the conversion efficiency of a real device, compared to predictions based on equation (3). More work is needed to find how the emission probability can be increased.

2.6. Validation and improvement of models

In contrast to the wide variety of models and simulation studies, the experimental data available for validation is still scarce. Some results have been presented for saturation current, or quantum yield, of PETE cathodes, but experimental data of power output and conversion efficiency of a complete device is still lacking. A good match of measured versus simulated internal QE is shown in figure 5(a) for a GaAs cathode with a hetero-structure barrier of height 0.22 eV at the emitting surface [16]. Most experimental results of PETE emission experiments are reported as normalized or arbitrary units, allowing qualitative and trend comparison versus models, but not a quantitative validation.

The elaborated model developed in [18] was also applied to the published experimental results [16]. The set of general transport equations (9)–(11) was solved in a 1D geometry corresponding to the experiment. The cathode has a three-layer hetero-structure with a 100 nm $Al_{0.4}Ga_{0.6}As$ electron blocking layer, 1 μm GaAs absorber layer, and a 70 nm $Al_{0.15}Ga_{0.85}As$ emitter layer that is activated with Cs at the external surface. All layers are doped 10^{18} cm^{-3} p-type. The cathode is illuminated from its emitting surface (reflection mode) and is biased such that all the emitted electrons reach the collector. The optical and properties of all materials were taken from the literature, including their dependence on temperature. The BSF layer contact is defined as a perfect Ohmic contact. The simulation models explicitly with finite thickness only the electron BSF and absorber layers. The emitting layer is modeled as a boundary condition with

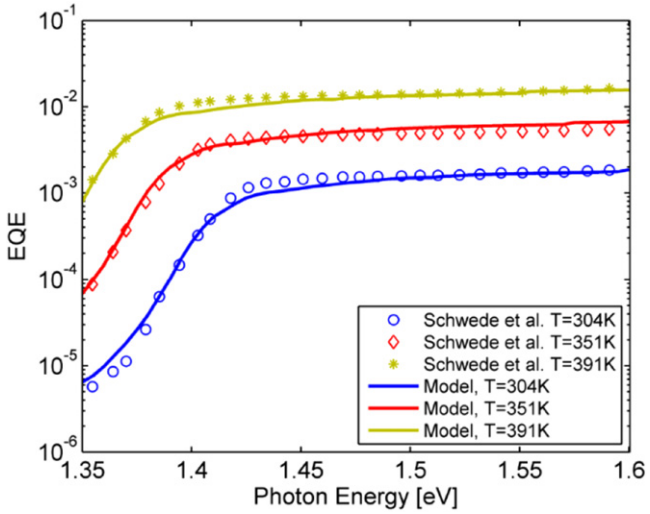

Figure 6. External quantum efficiency versus photon energy as calculated with the 1D model [18], versus experimental results published in [16].

electron emission and an effective surface recombination term. The emission barrier is determined by the absorber-emitter band offset and equals 0.22 eV. The effective surface recombination velocity was the only parameter left free to fit the experimental results, and the value that produced the best fit is $5 \cdot 10^5$ cm s^{-1} for both electron and holes. The simulation considered only photon energies below 1.6 eV (the bandgap of the emitting layer) to eliminate the effect of absorption in the emitting layer and photoemission from it that are present in the experiment. The external QE as a function of the incident photon energy at several temperatures is shown in figure 6 for the experiment and simulation. There is a very good fit between the two sets for the entire range of wavelengths and temperatures, indicating a successful quantitative validation of the model.

The performance predictions described above are based on some material properties that are realistic, but some other properties are assumed with optimistic values. For example, surface recombination velocities are sometimes assumed to be low or zero, the anode work function is assumed to be 0.5 eV or 0.6 eV in some cases, while the lowest known value for a real material is 0.9 eV [44], materials are analyzed in a temperature range that exceeds their range of stable operation, some properties are not known at high temperature, and extrapolated values are used without validation. Clearly this affects the reliability of the performance simulations, and requires additional effort to measure the missing data. The elaborated models published to date still rely on assumptions and simplifications, and could be improved for better correspondence to a real device. The treatment of optics is usually using single-pass exponential decay due to absorption, and does not contain a full description of non-collimated concentrated sunlight, and of photons created by radiative recombination. Heat transport and temperature gradients within the cathode, heat loss from the cathode to mechanical supports, conductors, and the anode, are neglected. A detailed treatment of coatings for electron affinity reduction, such as

polyscrystalline diamond films with complex morphology that affects their electronic properties, is absent. An IR absorber in the cathode is still used in models as an abstract notion without a definition of how it may be realized. A secondary thermal converter is often mentioned but the method to transport heat to the secondary converter, and its performance, were not analyzed in a realistic model. There is much more work then to improve the modeling of PETE conversion on all levels—from basic behavior of materials and components, to a better comprehensive treatment of a full converter device.

3. Materials and experimental results

3.1. Silicon cathode

Silicon is widely used in PV cells and therefore it is a natural candidate as a cathode material. However, its bandgap of 1.1 eV is far from the optimal bandgap for the absorption of sunlight, about 1.4 eV [4]. At elevated temperatures the bandgap will decrease even further, leading to a lower net voltage of the converter device and lower conversion efficiency. Nevertheless, there is research work performed on Si, both theoretically and experimentally, probably with the motivation that it is a readily available and well known semiconductor. Simulations with realistic properties of Si under 1000 suns have shown discouraging converter efficiencies of around 15% [14], 10% [21], and less than 15% for moderate cathode temperatures up to 800 K with a maximum efficiency of 30% at 850 K [18]. Differences among published predictions may be due to different models used to represent material properties. Experiments with both n-type and p-type Si with Cs coating [45] have demonstrated photonic enhancement of electron emission current. Experiments with Si coated by a low electron affinity hydrogen terminated diamond coating also showed the combined effect of illumination and heating [46], but did not clearly demonstrate if the absorption occurred in the Si or in the diamond film. All experiments to date provided only information regarding current, but no insight on conversion efficiency.

3.2. III-V cathode

The first experimental demonstration of PETE was done with a GaN cathode [4], which has a high bandgap and is not suitable as an absorber of solar energy. Other materials of the III-V family have a better match to the solar spectrum, most notably those that are currently in use for PV cells. GaAs and InP were considered as PETE cathodes, and simulations assuming high surface quality (low recombination) predicted efficiencies of 20%–25% at temperatures up to 900 K, with some advantage to InP [21]. An analysis for a GaAs cathode with a homo-junction at the contact instead of an unspecified high quality surface barrier predicted efficiencies below 20% for the same temperature range [18]. Cathode hetero-structures with GaAs/AlGaAs were also analyzed [19, 23] with some results exceeding 30% efficiency, depending on the level of optimism regarding surface quality. All of these studies stress the high impact of surface recombination and the need to minimize this effect in real devices. Some of these III-V materials are unstable at high temperatures above about 400 °C, while the long term stability of others is unknown. Ternary III-nitrides, which are more stable at high temperatures, can be adjusted to produce the needed bandgap, but these materials have not yet been considered for PETE cathodes. More research is therefore needed to determine which III-V materials could be good candidates for a PETE converter cathode. In addition to limitations on the cathode material, the electron emission surface of the cathode must be coated to reduce the electron affinity, but the coating also has temperature limitations, for example Cs on AlGaAs deteriorates already at 120 °C [16].

Experimental measurement of PETE yield from a GaAs cathode with a thin emission layer of $Al_{0.15}Ga_{0.85}As$ was done up to 120 °C, reaching a QE of 1.4% for 1.5 eV photons [16], much higher than the yield measured in previous work with GaN. The hetero-structure was designed to reduce recombination at the emission surface by introducing an internal surface with much higher quality, and an internal energy barrier at the conduction band, as shown in figure 7(a), allowing only energetic electrons to cross. Figure 7(b) shows the dependence of QE on temperature and photon energy, where photon energy above 1.64 eV produces a mix of PETE and photo-emission in both layers, while the range down to 1.42 eV is due only to PETE in the GaAs absorber. The PETE yield increases by an order of magnitude when the temperature increases to 120 °C, and the authors estimated that electrons excited in the GaAs absorber have a 7%–10% probability of crossing to the emitter layer, in spite of the energy barrier of 0.22 eV at the junction. The demonstrated improvement in QE is a promising step towards practical devices.

3.3. Diamond cathodes

The bandgap of diamond is too high and not suitable for the absorption of sunlight. However, a polycrystalline diamond film contains intermediate energy levels introduced by doping and grain boundaries, which enable the absorption of photons with much lower energy than the pure material bandgap [47]. For example, n-type doping with nitrogen creates states 1.7 eV below the conduction band minimum [48], an energy gap that is close to the bandgap needed for the effective absorption of sunlight. Diamond surfaces can also terminate with hydrogen to produce low or negative electron affinity [49]. The combination of these properties makes diamond an interesting candidate for PETE cathodes, either by itself, or as a thin film over a substrate. Electron emission from n-type diamond films over a metallic substrate under combined visible light illumination and heating showed a low effective work function of about 2 eV [50]. However, in this case the electrons are photo-excited in the metal, and then thermalize as they pass through the diamond film, which is somewhat different compared to PETE in a semiconductor substrate. Combined photoemission and PETE was observed with a

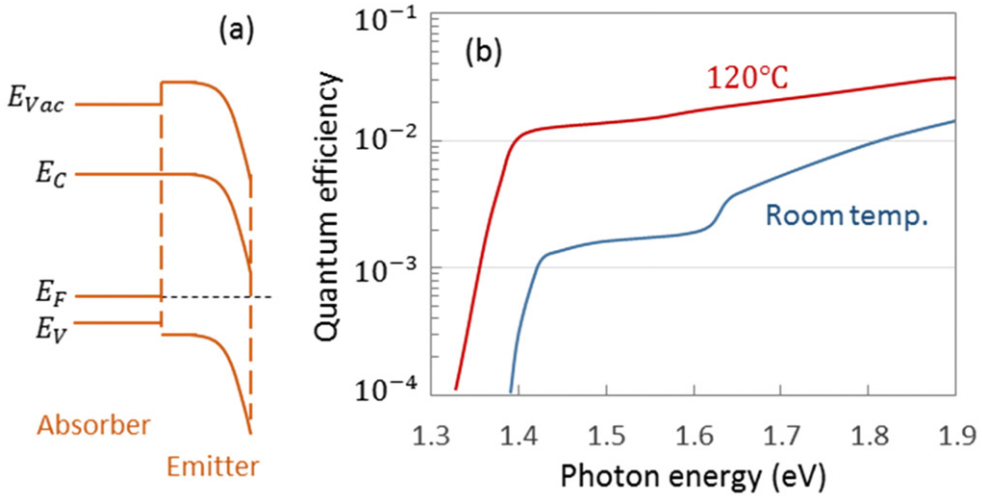

Figure 7. (a) Energy levels for a cathode with a GaAs absorber, $Al_{0.15}Ga_{0.85}As$ emitter with higher bandgap, and a Cs surface layer that creates near zero electron affinity. (b) Quantum efficiency of the structure, showing an order of magnitude increase in emission yield when temperature is increased to 120 °C, for illumination that is mostly absorbed in the GaAs main absorber layer. (Adapted from [16]).

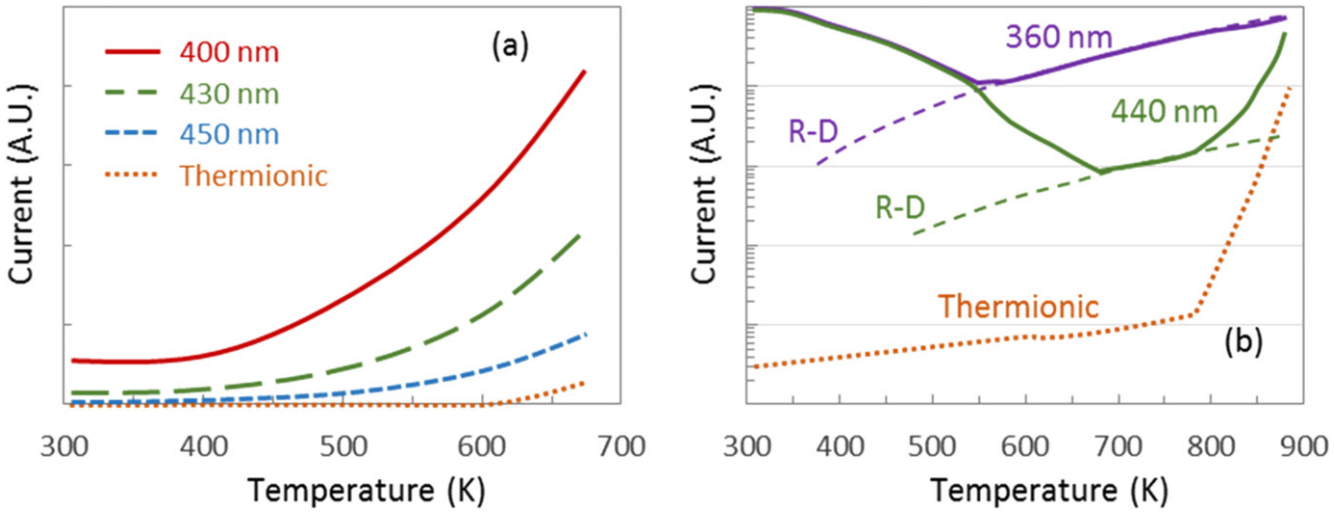

Figure 8. (a) Electron emission from n-doped diamond film over p-type Si substrate under heating and illumination at different wavelengths (adapted from [46]). (b) Electron emission from undoped diamond film over p-type Si substrate under heating and illumination at different wavelengths, with fits to the Richardson–Dushman (R–D) equation (adapted from [51]).

p-type Si substrate covered by an n-type nitrogen doped diamond film [46], as shown in figure 8(a). The dependence of the emission rate on incident photon energy at each temperature shows that the process is not pure PETE, and has a significant contribution of photoemission. Also, since illumination was through the diamond layer, it is difficult to separate the contribution of absorption and emission in the diamond versus the absorption in the Si substrate. Subsequent work [47] has shown that the absorption of visible light in the diamond, and resulting photo-excitation of electrons, are significant.

A different result is shown in electron emission measurements from undoped diamond film over p-type Si [51], as shown in figure 8(b). At low temperatures, photo-emission of electrons is dominant, and the yield decreases with temperature due to an increase in trap-assisted recombination and reduction of diffusion length. At moderate temperatures the behavior changes to increase with temperature, with a good fit to the Richardson–Dushman curve (dashed lines), showing that PETE is dominant in this range. In this work as well the behavior depends on the incident photon energy, in contrast with a simple description of PETE with full thermalization. The authors propose that transport of the generated electrons to the surface is the limiting factor due to the short diffusion length in polycrystalline diamond. The lower energy photons have a larger penetration depth before being absorbed, and are more influenced by this transport bottleneck. It is important to note that thermionic emission measurements of n-type CVD diamond films have shown an extremely low Richardson constant [39, 44], indicating that electron transport to the surface is a major issue that needs further investigation.

Absorption of sunlight in a polycrystalline diamond film is significant, but highly selective towards higher energy photons [47]. It is possible to increase absorption by modifying the surface of polycrystalline diamond with femtosecond laser pulses, creating ripples with controllable magnitude and spacing [52]. Absorptance of 0.8–0.9 was measured for the treated diamond in the wavelength range of 200–2000 nm, compared to <0.4 in most of this spectral range for the untreated material. This opens an interesting option for an all-diamond cathode, where both the absorber and the electron emission layer are made from the same material. However, it is still unclear how the introduction of such defects affects the electronic properties, in particular recombination rates and charge carriers transport.

3.4. Nanostructured cathodes

Electron emission properties can be significantly improved with the use of nanoscale surface features that modify locally the electronic behavior of the material. A survey of candidate structures that may reduce the effective surface work function and improve electron emission can be found in [8]. These include etched structures with nanoscale tips, carbon nanofibers and nanotubes, nano-wires, nano-crystalline diamond films, graphene films, etc. Surface structures with complex nanoscale geometry can also improve optical absorption, and almost complete absorption over a wide range of wavelengths and angles has been demonstrated, for example with 'forests' of carbon nanotubes [53]. Some of these structures have already shown promise in field emission and thermionic emission experiments, but very little work was reported for PETE. Recent work on carbon nanotubes [54] found that the variation with temperature of the electron emission current is qualitatively similar to the behavior expected of a PETE cathode. Also, evidence was found of two-photon photoelectron emission at moderate incident radiation flux, indicating that a nanotube forest can be more effective in the collection of excited electrons compared to a bulk metal cathode, where the two-photon effect occurs only at a very high radiation flux. However, the work function of carbon nanotubes is about 4.5 eV, too high for an effective electron emitter in a high efficiency converter. Performance of a CNT forest as an electron emitter may be improved by incorporating alkali metals, for example, potassium was shown to reduce the effective work function to about 2 eV at temperatures up to 600 K [55]. The area of surface nanostructures is very promising, very diverse, and mostly unexplored, with a high potential to offer major advances in the future.

3.5. Anode materials

The anode in a PETE converter seems less challenging than the cathode, but nevertheless there are two major requirements: its work function should be low to allow a significant net voltage of the device, and its resistance should be low to avoid Ohmic loss. A solution such as a metallic anode with a thin coating that creates a low effective work function, such as diamond, seems reasonable, and has demonstrated the lowest work function observed to date of 0.9 eV [44]. The Richardson coefficient, however, was very low (10^{-5} $Acm^{-2}K^{-2}$) indicating very high electrical resistance. A semiconductor with high n-type doping instead of a metal may also provide a good solution. The work function should not be too low, however, to prevent a significant reverse current from the anode to the cathode. A study for a GaAs cathode at 1000 K has shown that for each anode temperature, there is an optimal value of the anode work function [23]. For example, at anode temperatures of 400 K and 600 K, the optimal work function was 0.45 eV and 0.7 eV, respectively. This is not yet a practical issue, but it will become important if materials with a work function lower than 0.9 eV become available in the future.

4. Device and system aspects

4.1. Electrical contacts

The electrical contact at the cathode of a PETE converter presents an engineering challenge in two aspects: material and geometry. The contact material must be stable at high temperature, and must have very low diffusion into, and reaction with, the adjacent cathode material [56]. Its work function should match the cathode material electron affinity to avoid an energy barrier at the contact interface. The other contact at the anode is less problematic due to the lower temperature and no geometric constraints. Many metals have been considered for electrical contacts in high temperature electronics, which are usually based on SiC or III-nitrides, including nickel, tungsten, titanium, molybdenum, gold, palladium, and their alloys. There is limited work on the stability of such contacts after long exposure at high temperature: for example, Ni and Ni/Ti/Al alloy show good performance on SiC up to 500 °C [57]. However, some contact materials were found stable and others have degraded after 100 h at 700 °C [58]. The proposed mechanism to explain contact stability involves the formation of a silicide at the interface of the metal to the SiC substrate. This cannot apply to PETE cathodes made of other semiconductors, and specific semiconductor-metal combinations need to be tested.

The cathode contact geometry is important since placing contacts on the front surface will cause shading and loss of incident sunlight, similar to PV and CPV cells, as well as loss of electrons by recombination at the contact surface [18]. Placing electrical contacts at the back surface of the cathode will eliminate shading but also reduce the area for electron emission. In PV and CPV cells, the common solution is a contact grid at the front surface with area fraction and grid element distances optimized to reduce losses [59]. Some PV cells also have contacts at the back surface (back-contact cells). A schematic of a PETE converter with front and back contact grids is shown in figure 9(a).

The contact geometry for PETE Si cathodes was investigated for both front and back contacts, using a detailed 2D model [24]. Figure 9(b) shows that for moderate cathode temperatures, a smaller contact grid area is preferable. This is

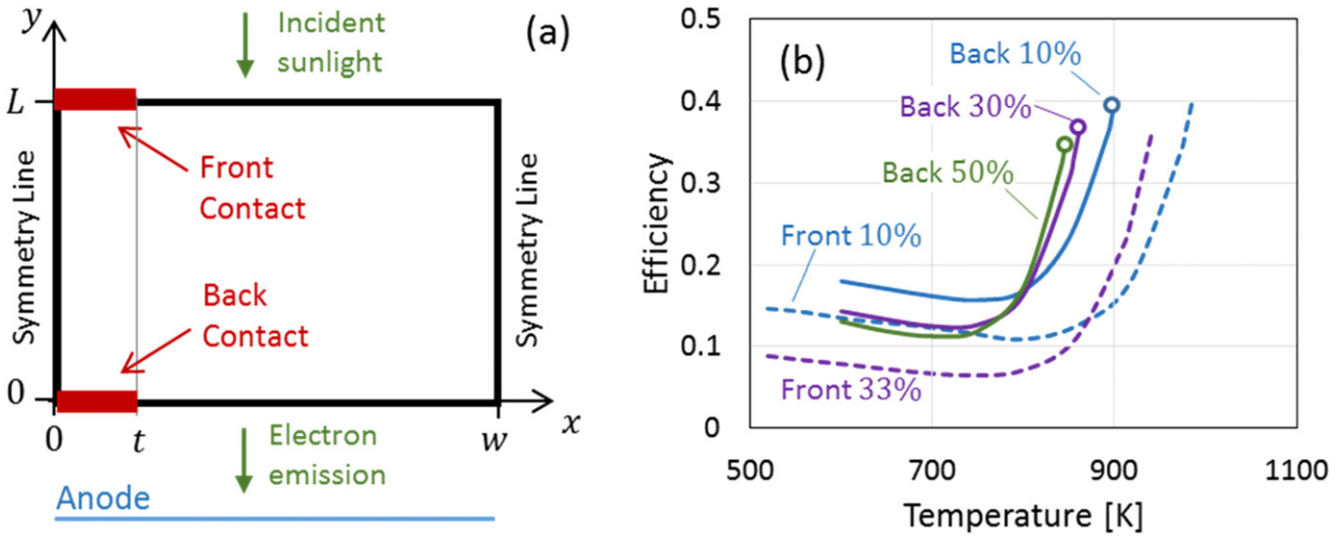

Figure 9. (a) Cross section of a PETE converter with a contact element location on the front and back surfaces. (b) Efficiency as a function of the cathode temperature for different sizes of back contact (solid lines) and front contact (dashed lines). Circles are the maximum achievable temperatures under ideal thermal balance (adapted from [24]).

due to the impact of shading (for the front contact) and contact recombination, which are dominant in this range. At high temperatures above 800 K, the trend is reversed and a larger contact area produces higher efficiency, for both the front and back contacts. Electron injection at the contact is responsible for this reversal, since at these temperatures the thermionic emission is dominant and the cathode is depleted in spite of the optical generation. Also note that in all cases the back contact efficiency is higher than the corresponding front contact of the same area. This indicates that the reduction in the area for electron emission at the back surface does not have a significant impact on performance. Another interesting option is to use the back contact in the role of absorber for sub-bandgap photons that traverse the absorber, a function that currently has no practical means for implementation. The back contact configuration should then be an excellent candidate for future PETE converter realization.

4.2. Window

The PETE converter should be enclosed and evacuated, while allowing incident radiation to enter and impinge on the cathode front surface. Therefore it must have an optical window adjacent to the cathode, or implemented as an additional layer of the cathode structure. Many of the cathode candidate materials require only a small thickness of the active material, a few microns or less, and therefore the window can serve as a substrate with sufficient mechanical strength to support the cathode. The window should then be stable at the high temperature of the cathode, leading to the selection of materials such as quartz or sapphire.

The window should include an anti-reflection coating to minimize reflection of incident sunlight, widely used in PV cells and other optical applications. However, the stability of available coatings must be verified under the high temperature. As an interesting alternative, a recent analysis found that a photonic crystal can improve the efficiency of a PETE converter by 20%, from 0.1 to 0.12, over a standard bilayer anti-reflective coating [20].

4.3. Thermal management and secondary converter

The anode of a PETE converter needs to be cooled in order to maintain a constant operating temperature. The main heat sources in the anode include: thermalization of electrons collected from the cathode, radiative heat transfer across the gap between the cathode and anode surfaces, and conduction heat transfer from the cathode through the device structure and encapsulation elements. If the cathode and anode surfaces are considered as parallel plates placed at a small distance compared to their lateral extent, the heat flux to be removed from the anode q_A can be approximately expressed as:

$$q_A = J_{net}\phi_{B,A} + \frac{T_C - T_A}{R_{th}} + \int_0^\infty \frac{e_{b\lambda}(\lambda, T_C) - e_{b\lambda}(\lambda, T_A)}{1/\epsilon_{\lambda,C}(\lambda) + 1/\epsilon_{\lambda,A}(\lambda) - 1}\mathrm{d}\lambda \qquad (12)$$

J_{net} is the net current density, $\phi_{B,A}$ is the potential difference between the anode conduction level and the highest vacuum potential in the gap including the effect of space charge [5], and their product is the anode thermalization power per unit area. R_{th} is the thermal resistance per unit area for conduction heat transfer between the cathode and anode, which depends on the structural design details of the device, and should be maximized by engineering optimization. $e_{b\lambda}$ is the blackbody spectral emission, $\epsilon_{\lambda,C}$ and $\epsilon_{\lambda,A}$ are the spectral emissivities of the cathode and anode surfaces, respectively, and the last term is then the total radiative flux between the two surfaces. A more detailed treatment, including additional secondary effects, such as Joule heating in the electrical conductors, and a distinction in thermal energy carried by electrons emitted from the cathode versus the anode, can be found in

[6]. If the gap size is around 1 μm or less, then near-field radiative heat transfer should be considered as well [35]. The emissivity of the two surfaces should be reduced as much as possible to reduce the radiative heat transfer mechanism. However, the ability to manipulate the optical property of the two surfaces may be limited due to the treatment of these surfaces to achieve the desired electronic properties (electron affinity/work function).

At the device level, the heat flux that needs to be removed from the anode of a PETE converter depends on the flux (concentration) of the radiation incident on the cathode, the converter operation point (current versus voltage), and the temperatures of both electrodes. Considering a converter operating under a concentration of 1000 suns, we estimate that about 50 W cm^{-2} needs to be removed from the anode, similar to the heat removal requirements for high-power electronic components [60] and for CPV cells that are subject to a similar concentration level. There are many common solutions for such components, and the applicability of these solution to the PETE anode should be considered.

An important consideration is whether the heat removed is to be exploited, or just removed to the ambient. For direct heat rejection, the preferred solution in CPV systems is passive cooling: the cell is mounted on a large area heat spreader plate made of a high thermal conductivity metal, copper or aluminum. Fins are added on the back surface of the plate, and the heat is removed by natural convection to the ambient air [61]. Such a solution can be used for the PETE anode, and it has been shown that under the given heat flux and the cell temperature excess the ambient temperature is <40 °C.

The waste heat removed from the anode can be used in a secondary stage, either to produce additional electricity in a secondary converter, or to be used as thermal energy input into other applications. Similar arrangements were proposed to exploit waste heat from CPV systems. The waste heat can drive a lower-temperature power generation converter such as an organic Rankine cycle or Stirling heat engine [62, 63]. Another power generation option without a mechanical engine is a thermoelectric converter, which usually offers lower efficiency but offers wide scalability and simple and robust operation [27]. Waste heat can also be used for other applications that do not generate electricity, such as the operation of an absorption chiller to produce cooling [64], and performing thermal desalination of seawater [65].

In order to enable secondary thermal applications, the anode temperature must be high enough for the thermal application to be effective. For example, an absorption chiller requires heat input at about 90 °C (single stage) or 150 °C (double stage); a heat engine requires heat input at 200 °C or higher in order to achieve reasonable efficiency. Fortunately, the PETE converter performance is not very sensitive to anode temperature due to the non-linear dependence of electron emission rate on temperature. Therefore, moderately high anode temperatures may be acceptable. In addition, waste heat removal should be based on active cooling: the anode should transfer the thermal energy to a heat transfer fluid (water, thermal oil, etc) that will carry the energy to the location of the secondary application. The thermal stage (heat engine, absorption chiller, etc) tends to be on a scale of kilowatts to tens or even hundreds of kW, while PETE converters probably will be on a scale of tens of watts, similar to CPV cells. Therefore, the thermal energy needs to be collected from many PETE converters and transported to a central thermal application. Many heat exchanger solutions exist for heat transfer from the anode back surface to a fluid, such as mini- and micro-channels, impingement and evaporative heat exchangers, and these are used for the cooling of various electronic components and of CPV cell arrays [61]. These heat exchangers provide effective heat transfer, but they may incur a high pressure drop (high pumping power). Therefore their implementation for a PETE anode cooler needs to be investigated and optimized carefully.

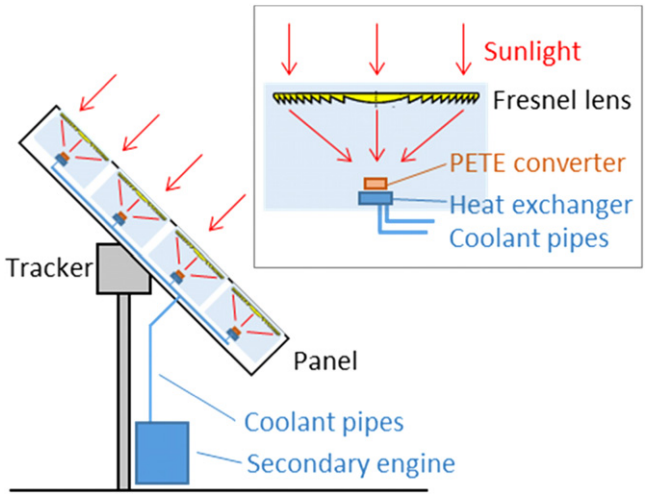

Figure 10. Schematic view of a PETE collector, containing many lens concentrators and PETE converters assembled on a panel that tracks to the direction of the Sun, and collecting heat via a coolant pipe network to a central secondary heat engine. Inset: magnified view of a single lens concentrating sunlight to a single PETE converter, a heat exchanger to remove heat from the anode, and pipes to provide coolant fluid and remove the hot fluid.

Figure 10 shows a schematic view of a PETE collector panel according to the general design of a CPV collector, and the considerations explained above: an array of Fresnel lenses concentrates solar radiation to an array of PETE converters. Each converter is installed on a heat exchanger that removes the waste heat from the anode to a working fluid. A pipe network collects the hot fluid to a central location, where the heat is used to drive a secondary heat engine.

4.4. Converter size

The selection of size for the PETE converter has many practical implications on the system level, with the influence, for example, on the type of concentration optics, on electrical wiring, on the mechanical arrangement of sun tracking, etc. The need for vacuum encapsulation, and the requirement for a small gap, are likely to limit the converter size, such that the active area exposed to concentrated solar radiation of a single converter could be a few millimeters to a few centimeters in diameter. This is similar to CPV cells, which today are made

at typical sizes of 5—10 mm. The leading concentration technology for CPV, Fresnel lenses, could then be suitable for PETE as well. CPV systems are typically made with arrays of lenses, each lens concentrating sunlight by a factor of 400–1000 to a single cell. A large array of lenses and corresponding cells is mounted on a single frame and is moved in two axes to track the direction of the Sun. This technology is well developed and demonstrated [1], and can be implemented for PETE converters with only a moderate effort for engineering integration. The alternative concentration technology, a dense array of converters with a single large concentrator [1], may have an advantage for easier collection of waste heat, but it may be difficult to pack together many PETE converters with minimal gaps when the converters have individual vacuum encapsulation.

The PETE converter size also determines the current output, which is important when considering the resistive (Ohmic) losses in the conductors attached to the converter. The converter has a typically low voltage, related to the difference in work function between the cathode and anode. Therefore its current can be high, similar to CPV cells that operate under high concentration. The issue of high Ohmic loss is usually resolved by increasing the cross section area of the conductors. However, in a PETE converter, one of the device conductors connects to the high temperature cathode. Increasing its cross section area will lead to increased heat loss by conduction from the cathode. The design of the electrical contact and related losses in the context of device and current size is then a significant issue that affects the device size and performance, and should be considered and optimized carefully.

5. Challenges and outlook

PETE offers an exciting new path to exploit electron emission phenomena for energy conversion, a goal that has been pursued over many decades with little success. Work done over the last five years has led to major advances in theoretical understanding and some first steps in the selection of materials and experimental verification. The most promising results come from the theoretical studies that show ideal performance limits equivalent and even surpassing the veteran approaches of photovoltaic and thermal conversion, and more realistic detailed modeling that shows efficiencies comparable to the best solar converters existing today. This serves as motivation to pursue the research of PETE conversion and the development of PETE converter technology. However, many challenges remain and much knowledge is still needed before this approach can materialize into proven technology and industrial application.

The most challenging aspect is finding a set of appropriate materials for the cathode, realizing that a single material probably cannot provide all the necessary functions: absorption of sunlight, efficient collection of charge carriers, and efficient emission of electrons. The materials set should also be defined with corresponding fabrication methods that can be upscaled to industrial production. Experimental work so far applies to a limited set of materials, and has a long way to go before achieving the yield and efficiency that are promised by the theoretical analyses. Also, some of these materials are already known to be unsuitable, for example, due to the inability to reach the high temperature required. However, recent advances in many materials—III–V semiconductors, diamond films, nanoscale structures in carbon and in other materials, and more—can open new directions for the implementation of PETE cathodes, beyond the obvious materials that have already been explored. A second, but equally important, challenge is the anode material, where the requirements of very low work function and low resistance are also waiting for better solutions.

In addition to the basic challenges in materials, many open issues can already be identified in device and system engineering for PETE converters. Fortunately, work over the last few decades on CPV cells and systems can provide many solutions, or at least insight on how to manage a device operating under intense concentrated sunlight. Not all device level issues can rely on CPV solutions and some challenges are unique to the thermionic world, such as vacuum encapsulation and mitigation of space charge. Much work is needed to develop practical configurations of PETE devices that simultaneously resolve all the difficulties.

The recent activities in PETE research have not yet produced a report of a working PETE device and a measured energy conversion efficiency. The demonstration of a working device is a crucial milestone in order to demonstrate that separate research on materials and components can be integrated successfully, and to validate the theoretical studies. Experimental results reported so far include emission currents and QE under a voltage bias, for example QE of 1.4% for in a cesiated GaAs cathode at 120 °C [16]. These are important first steps but are insufficient to evaluate the feasibility of full PETE conversion devices. Experimental demonstration of high efficiency approaching the theoretical predictions is then still a distant goal and needs a considerable period of intense research and development. If and when high efficiency is achieved, this will constitute a major advance in electron emission based energy conversion, and a possible contender in the solar electricity generation market.

Acknowledgments

This work was supported by the European Community FP7-Energy FET Project ProME^{3}ThE^{2}US^2, Grant Agreement n. 308975, (http://www.prometheus-energy.eu).

References

[1] Philipps S P and Bett A W 2014 III-V Multi-junction solar cells and concentrating photovoltaic (CPV) systems *Adv. Opt. Technol.* **3** 469–78
[2] Mancini T 2003 Dish-Stirling systems: an overview of development and status *J. Sol. Energy Eng.* **125** 135–51

[3] Smestad G 2004 Conversion of heat and light simultaneously using a vacuum photodiode and the thermionic and photoelectric effects *Sol. Energy Mater. Sol. Cells* **82** 227–40

[4] Schwede J W *et al* 2010 Photon-enhanced thermionic emission for solar concentrator systems *Nat. Mater.* **9** 762–7

[5] Segev G, Rosenwaks Y and Kribus A 2015 Limit of efficiency for photon-enhanced thermionic emission versus photovoltaic and thermal conversion *Sol. Energy Mater. Sol. Cells* **140** 464–76

[6] Hatsopoulos G N and Gyftopoulos E P 1973 *Thermionic Energy Conversion Volume I: Processes and Devices* (Cambridge, MA: MIT Press)

[7] Richardson O W 1912 Some applications of the electron theory of matter *Phil. Mag.* **23** 594–627

[8] McCarthy P T, Reifenberger R G and Fisher T S 2014 Thermionic and photo-excited electron emission for energy-conversion processes *Front. Energy Res.* **2** 1–15

[9] Hatsopoulos G N and Gyfopoulos E P 1979 *Themionic Energy Conversion, Volume II: Theory, Technology, and Applicaction* (Cambridge, MA: MIT Press)

[10] Houston J M 1959 Theoretical efficiency of the thermionic energy converter *J. Appl. Phys.* **30** 481

[11] Houston J M and Webster H J 1963 Thermionic energy conversion *Adv. Electron. Electron Phys.* **17** 125–206

[12] Shockley W and Queisser H J 1961 Detailed balance limit of efficiency of p-n junction solar cells *J. Appl. Phys.* **32** 510–9

[13] Segev G, Rosenwaks Y and Kribus A 2012 Efficiency of photon enhanced thermionic emission solar converters *Sol. Energy Mater. Sol. Cells* **107** 125–30

[14] Varpula A and Prunnila M 2012 Diffusion-emission theory of photon enhanced thermionic emission solar energy harvesters *J. Appl. Phys.* **112** 044506

[15] Sahasrabuddhe K, Schwede J W, Bargatin I, Jean J, Howe R T, Shen Z-X and Melosh N A 2012 A model for emission yield from planar photocathodes based on photon-enhanced thermionic emission or negative-electron-affinity photoemission *J. Appl. Phys.* **112** 094907

[16] Schwede J W *et al* 2013 Photon-enhanced thermionic emission from heterostructures with low interface recombination *Nat. Commun.* **4** 1576

[17] Su S, Zhang H, Chen X, Kang J and Chen J 2013 Parametric optimum design of a photon-enhanced thermionic solar cell *Sol. Energy Mater. Sol. Cells* **117** 219–24

[18] Segev G, Rosenwaks Y and Kribus A 2013 Loss mechanisms and back surface field effect in photon enhanced thermionic emission converters *J. Appl. Phys.* **114** 044505

[19] Yang Y, Yang W and Sun C 2015 Diffusion emission model for solid-state photon-enhanced thermionic emission solar energy converters *Mater. Sci. Semicond. Process.* **35** 120–6

[20] Buencuerpo J, Llorens M, Zilio P, Raja W, Cunha J, Alabastri A, Proietti R, Marti A and Versloot T 2015 Light-trapping in photon enhanced thermionic emitters *Opt. Express* **23** 1220–35

[21] Varpula A, Tappura K and Prunnila M 2015 Si, GaAs, and InP as cathode materials for photon-enhanced thermionic emission solar cells *Sol. Energy Mater. Sol. Cells* **134** 351–8

[22] Sze S M and Ng K K 2006 *Physics of Semiconductor Devices* 3rd edn (New York: Wiley)

[23] Yang Y, Yang W and Sun C 2015 Heterostructured cathode with graded bandgap window-layer for photon-enhanced thermionic emission solar energy converters *Sol. Energy Mater. Sol. Cells* **132** 410–7

[24] Sandovsky R, Segev G and Kribus A 2016 Investigation of contact grid geometry for photon-enhanced thermionic emission (PETE) solar converters *Sol. Energy J.* **133** 259–73

[25] Fletcher E A and Moen R L 1977 Hydrogen and oxygen from water *Science* (80-.) **197** 1050

[26] Vorobiev Y V, Gonzalez-Hernandez J and Kribus A 2006 Analysis of potential conversion efficiency of a solar hybrid system with high-temperature stage *J. Sol. Energy Eng.* **128** 258–60

[27] Su S, Wang Y, Wang J, Xu Z and Chen J 2014 Material optimum choices and parametric design strategies of a photon-enhanced solar cell hybrid system *Sol. Energy Mater. Sol. Cells* **128** 112–8

[28] Reck K and Hansen O 2014 Thermodynamics of photon-enhanced thermionic emission solar cells *Appl. Phys. Lett.* **104** 023902

[29] Segev G, Kribus A and Rosenwaks Y 2013 High performance isothermal photo-thermionic solar converters *Sol. Energy Mater. Sol. Cells* **113** 114–23

[30] Pozner R, Segev G, Sarfaty R, Kribus A and Rosenwaks Y 2011 Vertical junction Si cells for concentrating photovoltaics *Prog. Photovolt. Res. Appl.* **20** 197–208

[31] Smith J R, Bilbro G L and Nemanich R J 2009 Theory of space charge limited regime of thermionic energy converter with negative electron affinity emitter *J. Vac. Sci. Technol. B* **27** 1132

[32] Langmuir I 1923 The effect of space charge and initial velocities on the potential distribution and thermionic current between parallel plane electrodes *Phys. Rev.* **21** 419–35

[33] Su S, Wang Y, Liu T, Su G and Chen J 2014 Space charge effects on the maximum efficiency and parametric design of a photon-enhanced thermionic solar cell *Sol. Energy Mater. Sol. Cells* **121** 137–43

[34] Segev G, Weisman D, Rosenwaks Y and Kribus A 2015 Negative space charge effects in photon-enhanced thermionic emission (PETE) solar converters *Appl. Phys. Lett.* **107** 013908

[35] Lee J H, Bargatin I, Melosh N A and Howe R T 2012 Optimal emitter-collector gap for thermionic energy converters *Appl. Phys. Lett.* **100** 173904

[36] Lee J, Bargatin I, Vancil B K, Gwinn T O, Maboudian R, Melosh N A and Howe R T 2014 Microfabricated thermally isolated low work-function emitter *J. Microelectromech. Syst.* **23** 1–6

[37] Littau K A, Sahasrabuddhe K, Barfield D, Yuan H, Shen Z-X, Howe R T and Melosh N A 2013 Microbead-separated thermionic energy converter with enhanced emission current *Phys. Chem. Chem. Phys.* **15** 14442–6

[38] Ito T and Cappelli M A 2012 Optically pumped cesium plasma neutralization of space charge in photon-enhanced thermionic energy converters *Appl. Phys. Lett.* **101** 213901

[39] Koeck F A M, Nemanich R J, Balasubramaniam Y, Haenen K and Sharp J 2011 Enhanced thermionic energy conversion and thermionic emission from doped diamond films through methane exposure *Diam. Relat. Mater.* **20** 1229–33

[40] Meir S, Stephanos C, Geballe T H and Mannhart J 2013 Highly-efficient thermoelectronic conversion of solar energy and heat into electric power *J. Renew. Sustain. Energy* **5** 043127

[41] Smith J R, Bilbro G L and Nemanich R J 2006 Using negative electron affinity diamond emitters to mitigate space charge in vacuum thermionic energy conversion devices *Diam. Relat. Mater.* **15** (special issue) 2082–5

[42] Yang Y, Yang W, Tang W and Sun C 2013 High-temperature solar cell for concentrated solar-power hybrid systems *Appl. Phys. Lett.* **103** 083902

[43] Zhuravlev A G, Romanov A S and Alperovich V L 2014 Photon-enhanced thermionic emission from p-GaAs with nonequilibrium Cs overlayers *Appl. Phys. Lett.* **105** 251602

[44] Koeck F A M, Nemanich R J, Lazea A and Haenen K 2009 Thermionic electron emission from low work-function

phosphorus doped diamond films *Diam. Relat. Mater.* **18** 789–91
[45] Reck K, Dionigi F and Hansen O 2014 Photon-enhanced thermionic emission in cesiated p-type and n-type silicon *29th European Photovoltaic Solar Energy Conf. and Exhibition* pp 328–30
[46] Sun T, Koeck F A M, Rezikyan A, Treacy M M J and Nemanich R J 2014 Thermally enhanced photoinduced electron emission from nitrogen-doped diamond films on silicon substrates *Phys. Rev.* B **90** 121302
[47] Sun T, Koeck F A M, Stepanov P B and Nemanich R J 2014 Interface and interlayer barrier effects on photo-induced electron emission from low work function diamond films *Diam. Relat. Mater.* **44** 123–28
[48] Koeck F A M and Nemanich R J 2009 Low temperature onset for thermionic emitters based on nitrogen incorporated UNCD films *Diam. Relat. Mater.* **18** 232–4
[49] van der Weide J, Zhang Z, Baumann P K, Wensell M G, Bernholc J and Nemanich R J 1994 Negative-electron-affinity effects on the diamond (100) surface *Phys. Rev.* B **50** 5803–6
[50] Sun T, Koeck F A M, Zhu C and Nemanich R J 2011 Combined visible light photo-emission and low temperature thermionic emission from nitrogen doped diamond films *Appl. Phys. Lett.* **99** 202101
[51] Elfimchev S, Chandran M, Akhvlediani R and Hoffman A 2015 Trap-assisted photon-enhanced thermionic emission from polycrystalline diamond films *Phys. Status Solidi* **6** 1–6
[52] Calvani P, Bellucci A, Girolami M, Orlando S, Valentini V, Lettino A and Trucchi D M 2014 Optical properties of femtosecond laser-treated diamond *Appl. Phys.* A **117** 25–9
[53] Yang Z P, Ci L, Bur J A, Lin S Y and Ajayan P M 2008 Experimental observation of an extremely dark material made by a low-density nanotube array *Nano Lett.* **8** 446–51
[54] Vahdani Moghaddam M, Yaghoobi P, Sawatzky G A and Nojeh A 2015 Photon-impenetrable, electron-permeable: the carbon nanotube forest as a medium for multiphoton thermal-photoemission *ACS Nano* **9** 4064–9
[55] Westover T L, Franklin A D, Cola B A, Fisher T S and Reifenberger R G 2010 Photo- and thermionic emission from potassium-intercalated carbon nanotube arrays *J. Vac. Sci. Technol. B,* **28** 423
[56] Kolaklieva L and Kakanakov R 2009 Ohmic contacts for high power and high temperature microelectronics *Micro Electronic and Mechanical Systems* ed K Takahata (Rijeka: Intech)
[57] Smedfors K, Lanni L, Östling M and Zetterling C M 2013 Characterization of ohmic Ni/Ti/Al and Ni contacts to 4H-SiC from −40 °C to 500 °C *Silicon Carbide and Related Materials* **2013** 681–4
[58] Kakanakov R, Kasamakova-Kolaklieva L, Hristeva N, Lepoeva G, Gomes J B, Avramova I and Marinova T 2003 High temperature and high power stability investigation of Al-based ohmic contacts to p-type 4H-SiC *Mater. Sci. Forum* **457–460** 877–80
[59] Nishioka K, Takamoto T, Agui T, Kaneiwa M, Uraoka Y and Fuyuki T 2006 Evaluation of InGaP/InGaAs/Ge triple-junction solar cell and optimization of solar cell's structure focusing on series resistance for high-efficiency concentrator photovoltaic systems *Sol. Energy Mater. Sol. Cells* **90** 1308–21
[60] Kandlikar S G 2013 Review and projections of integrated cooling systems for 3D ICs *ASME J. Electron. Packag* **136** 1–11 no. June 2014
[61] Du D, Darkwa J and Kokogiannakis G 2013 Thermal management systems for Photovoltaics (PV) installations: A critical review *Sol. Energy* **97** 238–54
[62] Kribus A and Mittelman G 2008 Potential of polygeneration with solar thermal and photovoltaic systems *J. Sol. Energy Eng. Asme* **130** 011001-011001-5
[63] Kosmadakis G, Manolakos D and Papadakis G 2011 Simulation and economic analysis of a CPV/thermal system coupled with an organic Rankine cycle for increased power generation *Sol. Energy* **85** 308–24
[64] Mittelman G, Kribus A and Dayan A 2007 Solar cooling with concentrating photovoltaic/thermal (CPVT) systems *Energy Convers. Manag.* **48** 2481–90
[65] Mittelman G, Kribus A, Mouchtar O and Dayan A 2009 Water desalination with concentrating photovoltaic/thermal (CPVT) systems *Sol. Energy* **83** 1322–34